Programming light-harvesting efficiency using DNA origami

Elisa A. Hemmig,[†] Celestino Creatore,[†] Bettina Wünsch,[‡] Lisa Hecker,[‡] Philip Mair,[†] M. Andy Parker,[†] Stephen Emmott,[¶] Philip Tinnefeld,[‡] Ulrich F. Keyser,[*,†] and Alex W. Chin[*,†]

[†]*Cavendish Laboratory, University of Cambridge, Cambridge CB3 0HE, United Kingdom*

[‡]*Institut für Physikalische und Theoretische Chemie, TU Braunschweig, 38106 Braunschweig, Germany*

[¶]*Computational Science Laboratory, Microsoft Research, Cambridge CB1 2FB, United Kingdom*

E-mail: ufk20@cam.ac.uk; ac307@cam.ac.uk

Abstract

The remarkable performance and quantum efficiency of biological light-harvesting complexes has prompted a multidisciplinary interest in engineering biologically inspired antenna systems as a possible route to novel solar cell technologies. Key to the effectiveness of biological 'nanomachines' in light capture and energy transport is their highly ordered nanoscale architecture of photo-active molecules. Recently, DNA origami has emerged as a powerful tool for organising multiple chromophores with base-pair accuracy and full geometric freedom. Here, we present a programmable antenna array on a DNA origami platform which enables the implementation of rationally designed antenna structures. We systematically analyse the light-harvesting efficiency with respect to number of donors and inter-dye distances of a ring-like antenna using ensemble

and single-molecule fluorescence spectroscopy and detailed Förster modelling. This comprehensive study demonstrates exquisite and reliable structural control over multi-chromophoric geometries and points to DNA origami as highly versatile platform for testing design concepts in artificial light-harvesting networks.

Keywords

DNA nanotechnology, DNA origami, artificial light-harvesting, Förster resonance energy transfer, fluorescence spectroscopy

Biological light-harvesting complexes found in photosynthetic organisms efficiently capture solar photons by exploiting networks of precisely positioned chromophores. Such chromophore assemblies feed multiple electronic excitations into a single reactive centre via non-radiative Förster resonance energy transfer (FRET), leading to substantial absorption amplification. Energy transfer is further promoted by delocalised exciton states and quantum coherent transport. This allows the subsequent biochemical reactions, which are driven by electron-transfer events, to thrive even at ultra-low light conditions.[1,2] Although the underlying design principles of such natural photocells have been studied for over a century,[1] engineering synthetic analogues remains a formidable challenge.

The ability to use DNA as a template to arrange functional elements such as organic dyes[3–5] into specific arrays has undergone remarkable development over the last few decades. Recently, such chromophore-labelled DNA structures have been successfully employed to create photonic wires[5–7] and antenna systems,[8–11] marking the advent of DNA nanotechnology in the field of artificial photosynthesis. The programmed self-assembly of DNA has also inspired the development of structure-based computational models for light-harvesting applications.[12] Most of the studies so far, however, were performed using small DNA tile structures[8] or DNA constructs with flexible arms,[7] which, while establishing the crucial proofs of concept, are likely to suffer from low stability, sample heterogeneities, and struc-

tural uncertainties. With such high levels of variability in these structures, characterising their properties requires sophisticated single-molecule detection; successful engineering of a desired function cannot be easily inferred from ensemble measurements. Moreover, in many of these DNA-chromophore structures,[7] the light-harvesting topology is dictated by the underlying DNA template . This work demonstrates how many of these constraints can be removed by using programmable DNA origami structures to spatially co-ordinate dyes and effectively implement theoretical models of antenna systems in a highly robust and reproducible way.[12]

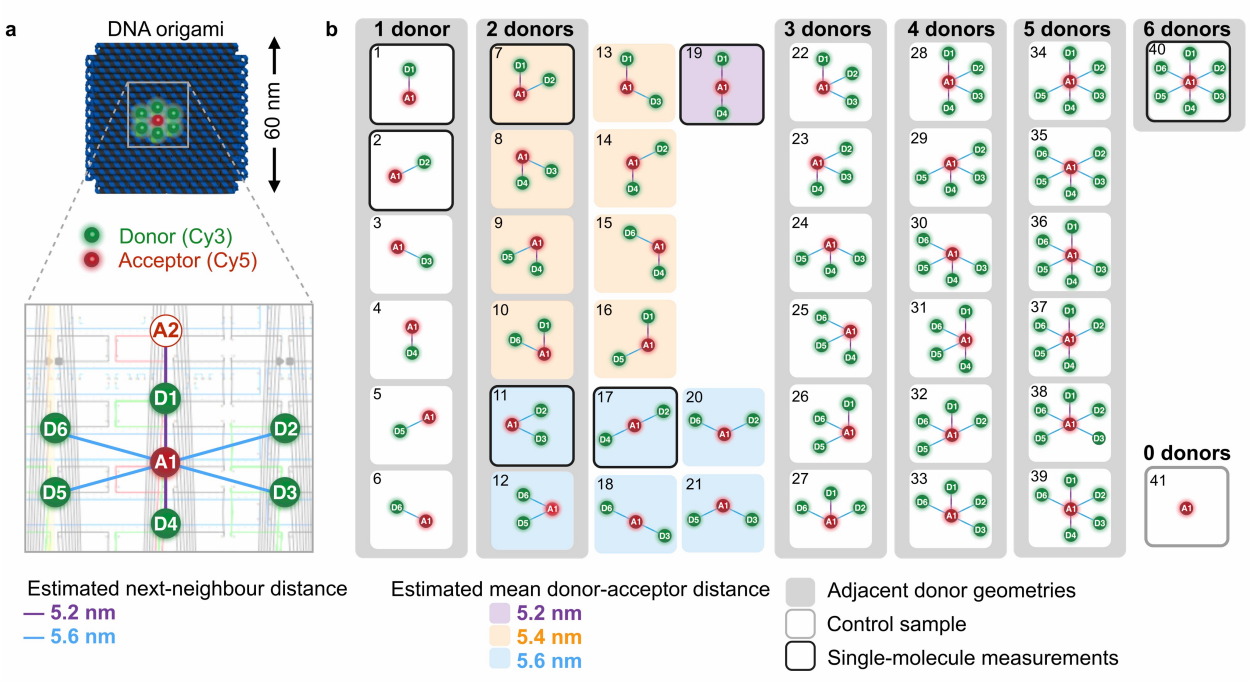

Figure 1: **Systematic design of DNA origami based donor-acceptor geometries. a)** A ring of Cy3 donor dyes (*green*) surrounds a Cy5 acceptor dye (*red*) on a flat, square-shaped DNA origami platform. The zoomed-in window shows the precise fluorophore attachment sites using a caDNAno scheme. **b)** For each number of donors N, we created all six permutations of adjacent donor positions (*grey* boxes) and prepared a control sample containing an acceptor only (*grey* frame). For $N = 2$, we assembled all the possible dye geometries resulting in three groups of different mean donor-acceptor distances (*coloured* boxes). The seven structures highlighted with *black* frames are analysed both in ensemble and single-molecule measurements.

The recent development of DNA origami based self-assembly[13,14] has enabled the fabrication of DNA nanostructures with significantly greater mechanical stability and rigidity.[15]

DNA origami structures are formed by folding a long, single-stranded piece of DNA ('scaffold') into a designed shape with the aid of hundreds of short, complementary 'staple' strands. Each staple is chemically addressable for functionalisation with fluorescent tags. To demonstrate how antenna designs can be implemented and analysed, we consider the problem of a single acceptor dye to which we progressively couple a number of donor dyes. For a set minimum donor-acceptor separation, we would expect that the total donor-acceptor energy transfer under FRET would be maximised by introducing each extra donor at this minimum separation; in 2D the optimal configuration would be a ring. Indeed, a circular ring of donors enclosing an acceptor (reaction centre) is a motif found in the (2D) photosynthetic membranes of purple bacteria.[16] To create this antenna geometry, we designed a two-layered DNA origami platform (54 nm $\times$ 60 nm), and selected 8 fluorophore attachment sites on this 'breadboard' so that the fluorophore is oriented away from the plane of the DNA platform. Six of these sites (Cy3 attachment) form a donor ring that surrounds a central acceptor site (Cy5 attachment). A further Cy5 attachment site is positioned outside the ring but equidistant from the nearest donor as the central acceptor. The well-defined DNA lattice allows us to estimate inter-chromophore distances using single-molecule measurements of the energy transfer efficiency of single donor-acceptor pairs. This yields distances of $\sim$ 5.2 nm in a perpendicular and $\sim$ 5.6 nm in a diagonal orientation with respect to helix direction (Fig. 1a and Supplementary Note S3). For this particular FRET pair (Cy3-Cy5) the Förster radius is $R_0 = 5.4$ nm:[17] the length scales of our platform are thus consistent with having FRET as the appropriate theory for energy transfer. At such inter-dye separations, the dyes are weakly coupled - the coupling being weak with respect to the homogeneous spectral line broadening. Hence, the transfer of the excitation energy between the donor and acceptor dyes can be correctly described within the FRET theory.[12,18,19] The detailed design, the protocols for assembly and purification, as well as the characterisation of the DNA origami platforms have been reported earlier.[20]

A key advantage of the DNA origami technique is its modularity; any of the fluores-

cently labelled staples can be simply replaced with their original, unmodified counterparts. Arbitrary combinations of fluorophores can therefore be programmed on the pre-defined positions on the DNA origami platform (see Supplementary Note S1 for DNA sequences of the modified staple strands and chemical structure of the dye attachment). Exploring this combinatorial freedom, we assembled over 30 structures by systematically varying the number of (adjacent) donors and permuting their positions (Fig. 1b). In the class of two-donor samples, we created all possible dye geometries yielding groups of different mean donor-acceptor distances (Fig. 1b). The DNA origami approach thus enables us to overcome the shortcomings of the antenna structures mentioned earlier[7] and explore the rational design of light-harvesting building blocks.

We begin with assessing the effectiveness of directional funnelling of excitation energy from the ring of donor molecules to the acceptor molecule in the centre. The acceptor molecule is positioned inside ('ring A_1') or outside ('ring A_2') the ring (Fig. 2a). Upon excitation of the donors, we observe a clearly enhanced fluorescence emission of the acceptor in 'ring A_1' as compared to 'ring A_2'. The fluorescence emission spectra of the control samples 'D_1-A_1' and 'D_1-A_2' are nearly identical (Fig. 2b), which confirms that the result of Fig. 2a is not induced by underlying structural differences of the DNA origami platform at these two acceptor positions. The excitation concentration observed in 'ring A_1' thus demonstrates the viability of our antenna system.

Building on this, we systematically study the light-harvesting efficiency of our DNA-based structures, which is quantified by the antenna effect (AE_{tot}).[21] This is defined as the ratio between the fluorescence of the acceptor upon excitation of donors [$I_A(D^*)$] to the fluorescence of the acceptor upon its direct excitation [$I_A(A^*)$] at given excitation wavelengths,

$$AE_{tot} = \frac{I_A(D^*)}{I_A(A^*)}\,. \tag{1}$$

The antenna effect quantifies the acceptor emission due to energy transfer from neighbouring donors relative to acceptor emission resulting from its direct excitation assuming equal

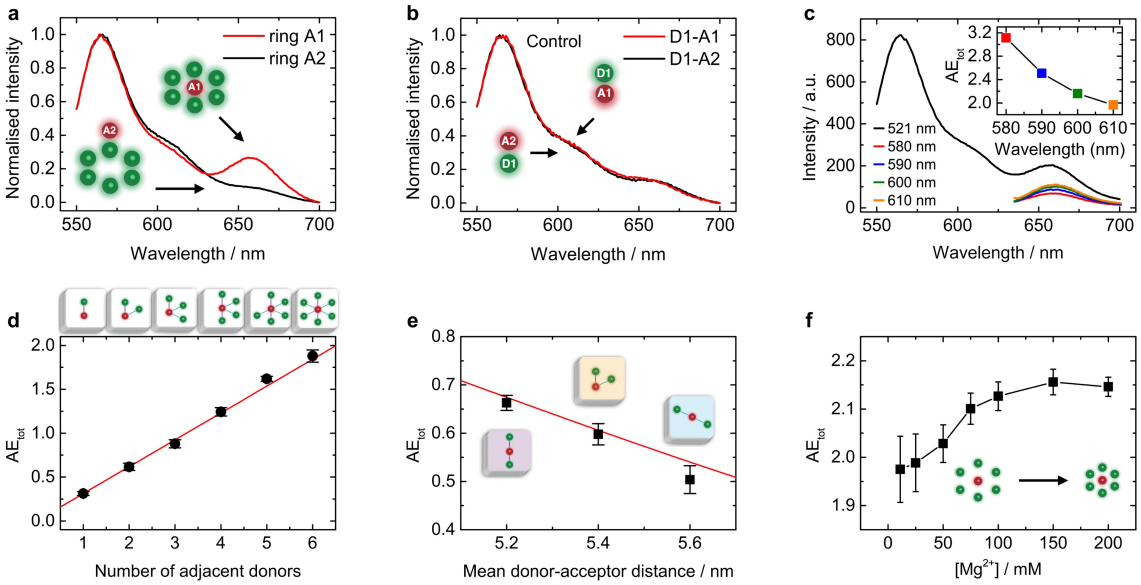

Figure 2: **Light-harvesting efficiency depends on donor-acceptor geometry. a)** Normalised fluorescence emission spectra with acceptor inside ('ring A_1', *red* line) and outside ('ring A_2', *black* line) the donor ring. **b)** Normalised fluorescence emission spectra of corresponding donor-acceptor pairs with donor fixed at D_1 and acceptor at A_1 ('D_1-A_1', *red* line) and at A_2 ('D_1-A_2', *black* line). **c)** Fluorescence emission spectra of the 6-donor ring with an acceptor in the centre when excited at different wavelengths. The *black* line corresponds to the emission when excited at the Cy3 (donor) excitation wavelength at 521 nm. The *coloured* lines correspond to the emission at direct Cy5 (acceptor) excitation at different wavelengths in the range 580–610 nm. *Inset*: Antenna effect (AE_{tot}) as a function of the acceptor excitation wavelength. **d)** AE_{tot} in dependence of number of adjacent donors N with linear fit (*red* line) according to Eq. (4). For each N, we averaged over all possible combinations of adjacent donors in the ring (Fig. 1b). The error bars correspond to the standard error of the mean. **e)** AE_{tot} as a function of mean donor-to-acceptor distance as determined from the two-donor samples (Fig. 1b). We prepared three independent replicates of each sample type. The error bars correspond to the standard error of the mean. The function (*red* line) shows the theoretical distance dependence of AE_{tot} (Eq. (5)). **f)** Influence of the concentration of Mg^{2+} ions in the buffer solution on AE_{tot} for the 6-donor ring with an acceptor in the centre. An increase in Mg^{2+} ion concentration is known to shrink the inter-helix distances in DNA origami structures[20]. We prepared three independent replicates of the sample. The error bars correspond to the standard error of the mean.

photon fluxes incident on both donor and acceptor dyes (see Supplementary Fig. S4 for more details on the analysis of the fluorescence emission spectra). It is important to highlight that the antenna effect is a parameter that can be tuned with the excitation wavelengths used. As shown in Fig. 2c, AE_{tot} decreases as the acceptor excitation wavelength approaches the absorption maximum of Cy5 (Supplementary Fig. S2) when the donor excitation wavelength is fixed.

We first analyse the antenna effect at an increasing number of donors N enclosing the common acceptor; for each donor number, AE_{tot} is obtained by averaging over all possible arrangements of adjacent donors within the ring (Fig. 1b). This approach ensures self-averaging of local donor-DNA and donor-acceptor interactions over the ring. For the fully occupied ring ($N = 6$), three replicates are prepared. Furthermore, AE_{tot} is corrected for direct excitation of the acceptor at the donor wavelength (521 nm) using a sample containing an acceptor only ($AE^0_{tot} \approx 0.08$), see Fig. 1b. We observe a linear increase of AE_{tot} with donor number N, which exceeds unity for $N > 3$ with a maximum value of $\sim$2 for $N = 6$ (Fig. 2d). This result implies that a higher total intensity of light is released by the acceptor dye following excitation of the donors (521 nm) than by direct excitation of the acceptor (600 nm). This is in good agreement with a theoretical analysis (see Model in Methods and the Supplementary Note S8) based on the solution of the rate equations of the excited state populations of donor and acceptor chromophores interacting via FRET, which predicts a linear scaling of AE_{tot} with number of donors N, see Eq. (4). Figure 2d shows how the experimental AE values are linearly fitted by Eq. (4), while in the Supplementary Note S7 we study the dependence of AE_{tot} on the number of donors without introducing any fitting parameters.

As expected, energy diffusion between the donors (homo-FRET) does not alter the net AE_{tot} in our dye configurations (see Model in Methods and Supplementary Note S8). In contrast to a homo-FRET based photonic wire,[10] the ring geometry ensures that all donors can effectively transport energy to the acceptor. Hence a circular antenna system consistently

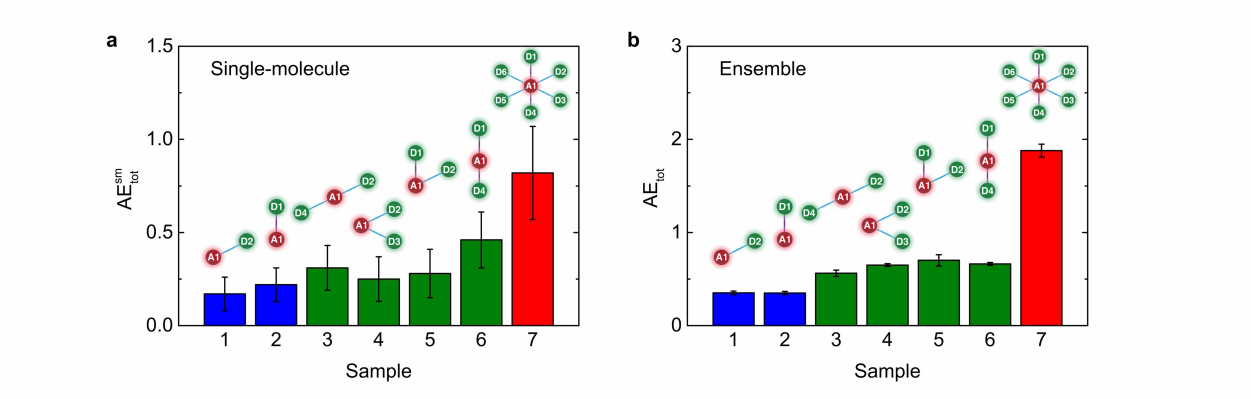

Figure 3: **Direct comparison between single-molecule and ensemble fluorescence measurements. a)** Antenna effect (AE_{tot}^{sm}) obtained from single-molecule measurements. We analysed 1-donor (*blue*), 2-donor (*green*) and 6-donor (*red*) samples (Fig. 1b). We screened several thousand molecules for each sample type, and used a Gaussian fit to determine the antenna effect. The error bars correspond to the standard deviation of the Gaussian fit. **b)** Antenna effect (AE_{tot}) obtained from ensemble measurements. We analysed 1-donor (*blue*), 2-donor (*green*) and 6-donor (*red*) samples (Fig. 1b). Each sample was prepared in three independent replicates. The error bars correspond to the standard error of the mean.

outperforms an equivalent linear array with the acceptor at one end, where the antenna effect is highly susceptible to weak links or disorder in the chain of dyes. Furthermore, AE_{tot} rapidly saturates as a function of N due to the inefficiency of the diffusive homo-FRET required to transfer energy across the array to the acceptor (see Supplementary Note S9).

Having understood the collective role played by the donors, we analyse how small changes in the donor-acceptor separation affect the light-harvesting efficiency of our antenna. We are able to vary the donor-acceptor separation in two fundamentally different ways; first, we can classify all possible two-donor configurations according to their mean donor-acceptor distance (Fig. 1b) as imposed by the anchoring positions on the DNA origami platform, which yields three different mean donor-acceptor distances (Fig. 1b). As shown in Fig. 2e, an increase in this distance by $\lesssim 1$ nm results in a substantial decrease of AE_{tot} by $\sim$23%. This is in agreement with the theoretical prediction given by Eq. (5). Second, we can dynamically tune the intrinsic compactness of a DNA origami structure and thereby the distances between the attached fluorophores by varying the concentration of Mg^{2+} ions in the buffer solution.[20] Increasing the concentration of Mg^{2+} ions leads to reduced inter-helix

distances due to electrostatic screening of the negatively charged DNA backbone. Indeed, as the $MgCl_2$ concentration is increased from 11 to 200 mM, AE_{tot} is enhanced by ∼9% for the full donor-ring antenna (see Fig. 2f and Supplementary Note S5 for more details).

As an essential part of testing new structures, we verify the results obtained in bulk using measurements of the antenna effect at single-molecule level for a sub-set of samples (Fig. 1b). The experimental setup applies alternating laser excitation (ALEX) of donor and acceptor fluorophores on diffusing molecules with separate donor and acceptor detection channels recording fluorescence bursts from single molecules (see Methods). This technique allows sorting of sub-populations and disregard molecules without FRET signal in the analysis. The quantity equivalent to AE_{tot} is defined as $AE^{sm}_{tot} = GR/RR$, where GR corresponds to 'green' excitation, 'red' detection, and RR to 'red' excitation, 'red' detection. We select representative samples with donor numbers $N = 1, 2, 6$ and measure the antenna effect both in single-molecule (Fig. 3a) and bulk (Fig. 3b) measurements (see Supplementary Note S6 for a comparison of energy transfer efficiency values). The overall trend – increasing antenna effect with donor number – is qualitatively reproduced in the single-molecule measurements. Furthermore, at a given donor number, we observe an increase in antenna effect with decreasing mean donor-acceptor distance (e.g. sample 3 vs. sample 6) (Fig. 3a). When averaging over all the values within a sample set with equal donor number ($N = 1, 2, 6$), the discrepancy in the mean values of AE_{tot} and AE^{sm}_{tot} can be clearly explained by the different excitation wavelengths used for the acceptor molecule in the respective experiment (see Fig. 2c and Supplementary Note S6 for a detailed explanation). Importantly, the single-molecule measurements show remarkably homogeneous populations for each sample indicating that all DNA origami structures have the same number of donors within our measurement accuracy (see the stoichiometry histograms in Supporting Note S6b). This gives us high confidence on the homogeneity and robustness of the DNA origami structures. In addition, the width of the homogenous populations of the antenna-effect (Fig. S6.1a) is mainly dominated by shot-noise and no significant conformational heterogeneity can be detected. The high quality

of samples and close agreement between the results obtained from both techniques thus allow the bulk measurements to be used as effective analytical tool.

To conclude, we have systematically built up a circular antenna system according to a rational design on a programmable material and with nanometre precision. Our rigorous and quantitative analysis has verified that the ring geometry functions effectively as an antenna. We have convincingly shown that DNA origami is a highly reliable tool for generating these antennas. Compared to DNA structures with flexible arms,[7] we have rigidified the system as inspired by protein scaffolds in real biological antennas; this promising avenue could be further explored using higher dimensional DNA origami architectures. Moreover, we have created a versatile platform for unravelling optimal energy transfer networks: By placing more dyes, such as multiple acceptors, we could investigate optimal donor-to-acceptor ratios or network geometries with multiple dye types, and even begin to replicate analogues of the energy transport system of entire photosynthetic membranes.

An intriguing future direction of this work is the possibility of engineering quantum effects that alter the fundamental nature of the antenna's photoexcitations. Recent theoretical work suggests that such effects could be exploited to enhance the performance of biologically inspired light-harvesting systems.[22–25] Quantum states, such as coherently coupled dimers, have already been realised in simple DNA duplexes,[26] but control over their spatial organisation proves to be challenging. The ability to program multi-chromophoric geometries using DNA origami could increase the complexity and connectivity of such quantum states, potentially creating an antenna operating beyond the classical regime.

Methods

Steady-state fluorescence measurements in bulk

Steady-state fluorescence emission was measured in bulk using a Cary Eclipse Fluorescence Spectrophotometer (Agilent Technologies) and a low volume cuvette (50 μl) (Sigma Aldrich).

Donor molecules (Cy3) were excited at 521 nm. Direct excitation of acceptor molecules (Cy5) was achieved using an excitation wavelength of 600 nm. The excitation and emission slits were set to 20 nm for the DNA origami samples (∼2 nM in 11 mM $MgCl_2$, buffered with 0.5 × TBE), and to 10 nm for the Cy3- and Cy5-labelled staple strands (∼500 nM in 1 × TE), respectively. Emission spectra were collected over a wavelength range of 550–700 nm upon excitation at 521 nm, and 635–700 nm upon excitation at 600 nm, respectively. For each sample, five fluorescence emission spectra were recorded and averaged for further analysis. The magnesium chloride titration was performed by stepwise addition of 1 M $MgCl_2$, buffered with 0.5 × TBE, to the same cuvette while recording the emission spectra.

Single-molecule fluorescence measurements

Single-molecule FRET measurements of individual diffusing DNA origamis were performed in LabTek chamber slides (Thermo Scientific) that were cleaned with 1 M KOH and passivated with BSA (10 mg/mL). Origamis were diluted in a buffer consisting of 1 × PBS, 12.5 mM $MgCl_2$ for stabilisation of the origami and 2 mM trolox/troloxquinone, 1%(w/w) glucose 10% (v/v) and 10% (v/v) of GOC (1 mg/mL glucose oxidase, 0.4% (v/v) catalase (50 μg/mL), 30% glycerol and 12.5 mM KCl in 50 mM TRIS pH 7.5) [27] for stabilisation of the fluorophores. Burst measurements were carried out on a custom-built confocal fluorescence microscopy setup. A diode laser with 80 MHz pulse frequency (640 nm, LDH-D-C-640, Picoquant) and a 532 nm cw laser (Sapphire LP 532 nm 100 mW, Coherent) were alternated by an acousto-optical tunable filter (AOTFnc-VIS, AA optoelectronic) with 100 μs period. The laser beams were coupled into an oil-immersion objective (UPlanSApo 60XO / 1.35 NA, Olympus) which is incorporated in an inverted microscope body (Olympus IX-71). The emission light was collected by the same objective and was separated from the excitation light by a dual-band dichroic beam splitter (z532/633 AHF) and focused onto a 50 μm pinhole (Linos). The emission of Cy3 and Cy5 was split spectrally by a single-band dichroic mirror (640 DCXR, AHF) and focused onto two avalanche photo diodes (τ-SPAD-100, Picoquant)

with appropriate filtering (Cy3 emission: Brightline HC582/75, AHF and RazorEdge LP 532, Semrock; Cy5 emission: Bandpass ET 700/75m, AHF and RazorEdge LP 647, Semrock). The detector signals were registered with a single photon counting PC card (SPC-830, Becker & Hickl) and evaluated using custom-made LabVIEW (National Instruments) software (see Supplementary Methods for details on data analysis).

Model

We modelled the energy transfer from the antenna complex to the common acceptor core using a set of rate equations governing the dynamics of the populations of the donor and acceptor chromophores, under external laser excitation and hetero-FRET interaction. This treatment assumes that only one particle, one excitonic quasiparticle in this case, is present in the system at any time and thus is fully valid to model the low-excitation conditions under which the experiments have been carried out.

For a single donor-acceptor pair, the antenna effect (AE_A^D) is given by (see Supplementary Note S8 for the full derivation):

$$AE_A^D = \frac{\Phi_D}{\Phi_A} E(R)\,, \tag{2}$$

where Φ_D (Φ_A) is proportional to the molar extinction coefficient of the donor (acceptor) dye $\Xi_D(\lambda_D)$ [$\Xi_D(\lambda_A)$] dependent on the excitation wavelength λ_D (λ_A) - see also S8, and $E(R)$ the FRET efficiency,

$$E(R) = R_0^6/(R_0^6 + R^6)\,, \tag{3}$$

with R_0 the Förster radius, i.e. the donor-acceptor separation corresponding to a FRET efficiency $E(R)$ equal to 50%.

When more than one donor is present, as in the ring antenna system examined here, the cumulative antenna effect (AE_{tot}) simply scales with the total number N of donor dyes D_i

$(i = 1, ..., N)$, if these are identical and located at a same distance from the acceptor A:

$$AE_{tot} = N\, AE_A^D\,. \tag{4}$$

In this case, we have not considered the homo-FRET interaction between identical donors. It can be demonstrated that the energy transfer between identical dyes located at the same distance from the common acceptor does not alter the net antenna effect (Supplementary Note S8).

For two donors D_1 and D_2 nearly equally spaced from the common acceptor A with distances R_1 and R_2, respectively, we can introduce an average donor-acceptor separation $\bar{R}$ so that $R_1 = \bar{R} + \delta R \gtrsim R_2 = \bar{R} - \delta R$. In this case, the cumulative antenna effect, $AE_A^{D_1} + AE_A^{D_2}$ can be expressed in terms of $\bar{R}$ (see also Supplementary Note S10):

$$\begin{aligned} AE_{tot}(\bar{R}) &= \frac{\alpha}{1+\beta(\bar{R}+\delta R)^6} + \frac{\alpha}{1+\beta(\bar{R}-\delta R)^6} \approx \\ & \frac{2\alpha}{1+\beta\bar{R}^6} + O(\delta R^2)\,, \end{aligned} \tag{5}$$

where $\alpha = \Phi_D/\Phi_A$ and $\beta = 1/R_0^6$.

We have used the experimental efficiencies measured by single-molecule spectroscopy (Supplementary Fig. S3), to evaluate the two distinct donor-acceptor distances ($D1$-A and $D2$-A). Using Eq. (3) with a Förster radius $R_0 = 5.4$ nm,[17] we get $R_{D_1A} = 5.2$ nm and $R_{D_2A} = 5.6$ nm.

The experimental values of the antenna effect as a function of the number of donors (Fig. 2d) have been fitted using Eq. (4). In this case we have assumed an average donor-acceptor efficiency $E(\bar{R})$, $\bar{R} = (R_{D_1A} + R_{D_1A})/2$ (see Supplementary Note S10) and fitted the experimental antenna effects (y) with the linear expression $y = \tilde{\alpha}x + q$, $x = NE(\bar{R})$ $(N = 1, ..., 6)$ and $\tilde{\alpha} = \Phi_D/\Phi_A$. From the linear fit we get $\tilde{\alpha} = \Phi_D/\Phi_A = 0.606$ and $q = 0.006$. Then, with $\tilde{\alpha}$ obtained from the linear fit and using $R_0 = 5.4$ nm, we compare the

theoretical antenna effect Eq. (5) evaluated as a function of the donor-acceptor separation (in the two-donor configuration) with the experimental values (see Fig. 2e).

Associated Content

Supporting Information Available

DNA origami design, fluorophore arrangement and attachment, spectroscopic properties of Cy3 and Cy5, energy transfer efficiency of single donor-acceptor pairs, calculation of antenna effect in ensemble fluorescence measurements, magnesium dependent fluorescence quenching, histograms from single-molecule fluorescence measurements, comparison of antenna effect and energy transfer efficiency between single-molecule and ensemble measurements, detailed derivation of model and further theoretical considerations, and supplementary methods. This material is available free of charge via the Internet at `http://pubs.acs.org/`.

Author Information

Author Contributions

M. A. P. and S. E. initiated the project. U. F. K. and A. W. C. conceived the work. U. F. K. and E. A. H. designed the experiments. E. A. H. and P. M. prepared the DNA origami samples, performed the ensemble spectroscopic measurements and analysed the data. B. W. and L. H. performed the single-molecule spectroscopic measurements on the DNA origami samples and analysed the related data. P. T. supervised the single-molecule measurements. A. W. C. and C. C. performed the simulations based on Förster theory used to model the experimental data. E. A. H. and C. C. wrote the manuscript with inputs from all authors.

Notes

The authors declare no competing financial interests.

Acknowledgement

A. W. C. acknowledges support from the Winton Programme for the Physics of Sustainability. U. F. K. was partly supported by an ERC starting grant (PassMembrane, EY 261101). E. A. H. acknowledges support from Janggen-Pöhn Stiftung and the Schweizerischer Nationalfonds (SNF). P. T. acknowledges support by a starting grant (SiMBA, EU 261162) of the European Research Council (ERC). B. W. gratefully acknowledges support by the Braunschweig International Graduate School of Metrology B-IGSM and the DFG Research Training Group GrK1952/1 'Metrology for Complex Nanosystems'. P. M. thankfully acknowledges the support of the EPSRC Centre for Doctoral Training in Sensor Technologies and Applications EP/L015889/1.

References

(1) Blankenship, R. E. *Molecular Mechanisms of Photosynthesis*; Blackwell Science Ltd, 2008.

(2) Scholes, G. D.; Fleming, G. R.; Olaya-Castro, A.; van Grondelle, R. *Nature Chemistry* **2011**, *3*, 763–774.

(3) Heller, M. J.; Tullis, R. H. *Nanotechnology* **1991**, *2*, 165.

(4) Stein, I. H.; Schüller, V.; Böhm, P.; Tinnefeld, P.; Liedl, T. *ChemPhysChem* **2011**, *12*, 689–695.

(5) Stein, I. H.; Steinhauer, C.; Tinnefeld, P. *Journal of the American Chemical Society* **2011**, *133*, 4193–4195.

(6) Hannestad, J. K.; Sandin, P.; Albinsson, B. *Journal of the American Chemical Society* **2008**, *130*, 15889–15895.

(7) Buckhout-White, S.; Spillmann, C. M.; Algar, W. R.; Khachatrian, A.; Melinger, J. S.; Goldman, E. R.; Ancona, M. G.; Medintz, I. L. *Nature Communications* **2014**, *5*.

(8) Dutta, P. K.; Varghese, R.; Nangreave, J.; Lin, S.; Yan, H.; Liu, Y. *Journal of the American Chemical Society* **2011**, *133*, 11985–11993.

(9) Albinsson, B.; Hannestad, J. K.; Börjesson, K. *Coordination Chemistry Reviews* **2012**, *256*, 2399–2413.

(10) Woller, J. G.; Hannestad, J. K.; Albinsson, B. *Journal of the American Chemical Society* **2013**, *135*, 2759–2768.

(11) Dutta, P. K.; Levenberg, S.; Loskutov, A.; Jun, D.; Saer, R.; Beatty, J. T.; Lin, S.; Liu, Y.; Woodbury, N. W.; Yan, H. *Journal of the American Chemical Society* **2014**, *136*, 16618–16625.

(12) Pan, K.; Boulais, E.; Yang, L.; Bathe, M. *Nucleic Acids Research* **2014**, *42*, 2159–2170.

(13) Rothemund, P. W. K. *Nature* **2006**, *440*, 297–302.

(14) Castro, C. E.; Kilchherr, F.; Kim, D.-N.; Shiao, E. L.; Wauer, T.; Wortmann, P.; Bathe, M.; Dietz, H. *Nature Methods* **2011**, *8*, 221–229.

(15) Liedl, T.; Högberg, B.; Tytell, J.; Ingber, D. E.; Shih, W. M. *Nature Nanotechnology* **2010**, *5*, 520–524.

(16) Hu, X.; Damjanović, A.; Ritz, T.; Schulten, K. *Proceedings of the National Academy of Sciences* **1998**, *95*, 5935–5941.

(17) Lee, S.; Lee, J.; Hohng, S. *PloS one* **2010**, *5*, e12270.

(18) Khan, Y. R.; Dykstra, T. E.; Scholes, G. D. *Chemical Physics Letters* **2008**, *461*, 305–309.

(19) Olaya-Castro, A.; Scholes, G. D. *International Reviews in Physical Chemistry* **2011**, *30*, 49–77.

(20) Li, C.-Y.; Hemmig, E. A.; Kong, J.; Yoo, J.; Hernández-Ainsa, S.; Keyser, U. F.; Aksimentiev, A. *ACS Nano* **2015**, *9*, 1420–1433.

(21) Brousmiche, D. W.; Serin, J. M.; Fréchet, J. M. J.; He, G. S.; Lin, T.-C.; Chung, S.-J.; Prasad, P. N.; Kannan, R.; Tan, L.-S. *The Journal of Physical Chemistry B* **2004**, *108*, 8592–8600.

(22) Creatore, C.; Parker, M. A.; Emmott, S.; Chin, A. W. *Physical Review Letters* **2013**, *111*, 253601.

(23) Higgins, K. D. B.; Benjamin, S. C.; Stace, T. M.; Milburn, G. J.; Lovett, B. W.; Gauger, E. M. *Nature Communications* **2014**, *5*, 4705.

(24) Zhang, Y.; Oh, S.; Alharbi, F. H.; Engel, G. S.; Kais, S. *Physical Chemistry Chemical Physics* **2015**, *17*, 5743–5750.

(25) Creatore, C.; Chin, A. W.; Parker, M. A.; Emmott, S. *Frontiers in Materials* **2015**, *2*, 6.

(26) Asanuma, H.; Fujii, T.; Kato, T.; Kashida, H. *Journal of Photochemistry and Photobiology C: Photochemistry Reviews* **2012**, *13*, 124–135.

(27) Cordes, T.; Vogelsang, J.; Tinnefeld, P. *Journal of the American Chemical Society* **2009**, *131*, 5018–5019.

List of changes

Graphical TOC Entry